

# Vibration Dependent Branching and Photoelectron Angular Distributions Observed across the Cooper Minimum Region of Bromobenzene

Ivan Powis\*

*School of Chemistry, University of Nottingham, Nottingham NG7 2RD, UK*

Minna Patanen,<sup>†</sup> Egill Antonsson,<sup>‡</sup> Christophe Nicolas, and Catalin Miron<sup>§</sup>

*Synchrotron SOLEIL, l'Orme des Merisiers, Saint-Aubin, BP 48, 91192 Gif-sur-Yvette Cedex, France*

David M. P. Holland

*Daresbury Laboratory, Daresbury, Warrington, Cheshire WA4 4AD, UK*

(Dated: June 15, 2017)

Vibrational state-resolved photoelectron anisotropy parameters,  $\beta$ , for the  $\tilde{X}^2B_1$ ,  $\tilde{B}^2B_2$ , and  $\tilde{C}^2B_1$  state ionizations of bromobenzene have been recorded at photon energies ranging from 20.5 to 94 eV, so spanning the region of the expected bromine Cooper minimum (CM). The  $\tilde{X}$  state displays no CM and its  $\beta$  value is also independent of vibrational level, in accord with the Franck-Condon Approximation. The  $\tilde{B}$  and  $\tilde{C}$  state  $\beta$  values display the CM to differing degrees, but both show a vibrational dependence that extends well below the obvious CM dip. Calculations are presented that replicate these observations of Franck-Condon Approximation breakdown spanning an extended photon energy range. This is the first demonstration of such wide-ranging breakdown detected in the  $\beta$  anisotropy parameter in the absence of any resonance. Measured and calculated vibrational branching ratios for these states are also presented. Although the  $\tilde{B}$  state branching ratios remain constant, in accord with Franck-Condon expectations, the  $\tilde{X}$  and (especially) the  $\tilde{C}$  state ratios display weak, quasi-linear variations across the studied range of photon energy, but with no apparent correlation with the CM position.

## I. INTRODUCTION

The concept of the Cooper minimum is long-established in the context of valence photoionization cross-section studies, but is receiving fresh attention in the investigation of high harmonic generation (HHG)[1]. In HHG the recollision of the laser field-driven electron can be considered an inverse photoemission and so the Cooper minimum can be imprinted on the HHG spectral profile. As originally proposed [2] the Cooper minimum occurs in atomic ionization when the initial orbital possesses a radial node and the electric dipole matrix elements can be considered an  $r$ -weighted overlap integral this orbital forms with the outgoing  $\Delta l = \pm 1$  waves. As the electron energy increases, and the outgoing waves contract towards the core, the overlap integral in a given channel can change sign, the relevant matrix element consequently passing through a zero. At this point there will be a corresponding minimum in the total photoionization cross-section.

The atomic photoelectron angular distribution can be even more strongly influenced by a Cooper minimum (CM) than is the cross-section. Again this is readily understood in the atomic-like picture; for photoionization of a  $3p$  electron there will be outgoing  $s$ - and  $d$ - waves, and as  $3p \rightarrow kd$  amplitude gets cancelled at the CM, the isotropic  $s$ -wave alone remains to dominate, with the  $\beta$  anisotropy parameter consequently dipping to zero. In practice, however, the observed minima of cross-section and  $\beta$  parameter may not exactly coincide [3].

The CM is also well established as a molecular phenomenon [4]. Most effort has been expended on identifying those instances of atomic-like behaviour that can be associated with lone pair electrons localized on heavy atoms with, again, parallels in the context of current HHG developments [5]. While halogen containing species have been at the heart of many such early investigations [4, 6], other embedded heavy atoms such as S and Se have been examined [7]. Phenomenologically, the depth of a molecular CM, or even its absence, can be used to infer the degree to which atomic character of the initial orbital is suppressed by the mixing in of more delocalized molecular orbitals. This can be thought of as an initial state effect. At the same time the non-central molecular potential scatters the outgoing electron into a greater range of outgoing channels with different phases, so that more complex interchannel interferences arise which are no longer just simple attenuation of a single channel. As a final state effect these interferences are reflected in the experimental observables such as depth and position of a CM, underscoring requirements for more fully developed theoretical understanding. For these more complex non-

\* ivan.powis@nottingham.ac.uk

<sup>†</sup> Current Address : Nano and Molecular Systems Research Unit, Molecular Materials Research Community, Faculty of Science, P.O.Box 3000, 90014 University of Oulu, Finland

<sup>‡</sup> Current Address : Institut für Chemie und Biochemie - Physikalische und Theoretische Chemie, Freie Universität Berlin, Takustr. 3, D-14195 Berlin, Germany

<sup>§</sup> Current Address: Extreme Light Infrastructure-Nuclear Physics (ELI-NP), "Horia Hulubei" National Institute for Physics and Nuclear Engineering, 30 Reactorului Street, RO-077125 Măgurele, Jud. Ilfov, Romania.

61 central potential cases the angular distribution provides  
62 the favoured CM diagnostic marker.

63 The outer valence orbitals of bromobenzene provide  
64 an interesting opportunity to examine molecular CM ef-  
65 fects. The outermost benzene  $\pi$ -type orbitals are split,  
66 by the  $C_{2v}$  symmetry, into a  $5b_1$  and  $2a_2$  pair. The next-  
67 lying atomic Br  $4p$  lone pair likewise splits into individ-  
68 ual  $8b_2$  and  $4b_1$  orbitals lying, respectively, in- and out-  
69 of the molecular plane and these can therefore interact  
70 in different degrees with the benzene ring electron den-  
71 sity. One thus anticipates finding in these orbitals ex-  
72 amples of either no-, strong-, or partial- localization at  
73 the Br atom [8] and the  $\beta$ -parameters associated with  
74 these outer four electronic bands in the photoelectron  
75 spectrum (PES) have been measured over extended pho-  
76 ton energies (ranging up to 94 eV [9] or 120 eV [10])  
77 to reveal modified molecular CM. Their interpretation  
78 clearly reflects these differences in localization and the  
79 one-particle, molecular orbital model for ionization holds  
80 well in these cases [8, 10].

81 A different class of CM, with an intrinsically molec-  
82 ular origin, has also been identified in lighter molecules  
83 such as small hydrides [11, 12], NO [13], and  $N_2$  [14].  
84 Since both initial and/or final state effects may be in-  
85 fluenced by the molecular environment, a novel vibra-  
86 tional sensitivity was predicted in the vicinity of the CM  
87 in OH [12]. Subsequently, pioneering studies by Poli-  
88 akoff and co-workers [15] have examined the dependence  
89 of the vibrational branching ratios through the  $N_2$   $2\sigma_u^{-1}$   
90 Cooper minimum. In the absence of resonant processes,  
91 such as autoionization and shape resonances, the Franck-  
92 Condon (FC) approximation predicts that vibrationally  
93 resolved branching ratios would be independent of elec-  
94 tron (photon) energy. However, these experiments and  
95 modelling [15] showed a slow but definite variation of vi-  
96 brational branching ratios, occurring over an extended  
97 excitation range of several tens of eV through the CM,  
98 and were interpreted as providing evidence for a wide-  
99 ranging, non-resonant FC violation.

100 The FC assumption of fully decoupled electron and  
101 nuclei motions also leads to a prediction that vibra-  
102 tionally resolved photoelectron anisotropy parameters  
103 should display an energy dependence that was indepen-  
104 dent of vibrational state. In this paper we seek, by mea-  
105 suring vibrationally resolved  $\beta$  anisotropy parameters  
106 and branching ratios, to further explore FC limitations  
107 while avoiding shape- and autoionizing resonances. Re-  
108 cent high resolution photoelectron studies of bromoben-  
109 zene [9, 16] have revised and extended the earlier vibra-  
110 tional analysis[10] of the outer valence bands. We now  
111 exploit the high resolution achievable at the PLÉIADES  
112 beamline (Synchrotron SOLEIL) to track the photoion-  
113 ization of these bands, maintaining full vibrational reso-  
114 lution across the extended photon energy range 20.5 to 94  
115 eV. By recording angle-resolved PES we are able, for the  
116 first time, to extract vibrationally resolved  $\beta$  parameters  
117 completely spanning a molecular CM region.

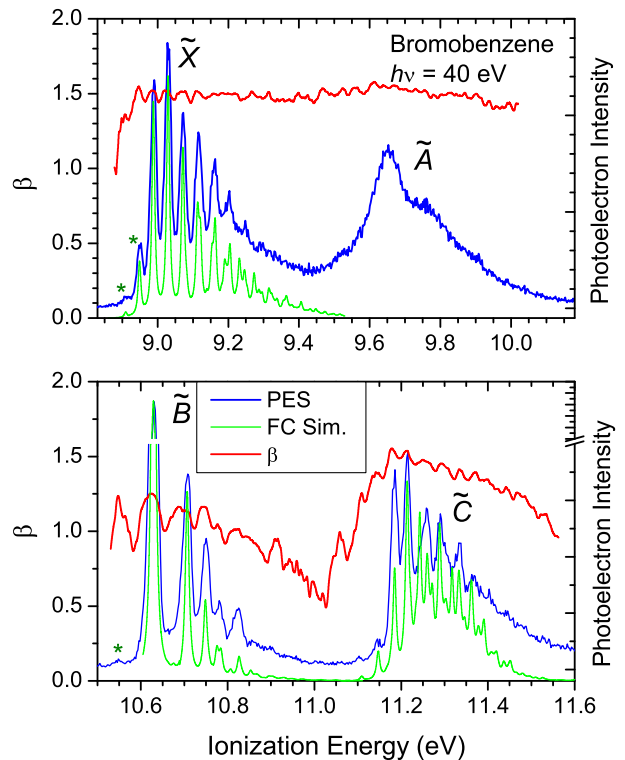


FIG. 1. Overview of the  $h\nu = 40$  eV data. The “magic angle” photoelectron spectrum is reconstructed by combining scans recorded with parallel and perpendicular linearly polarized light and the  $\beta$  parameter trace is similarly constructed from these recordings. Note the break in the vertical axis to truncate the intense origin of the  $\tilde{B}$  band. A Franck-Condon simulation (Ref. 9) is also shown with a small vertical offset for the vibrationally well-resolved  $\tilde{X}$ ,  $\tilde{B}$ , and  $\tilde{C}$  bands. Features assigned as vibrational hot bands are starred.

## 118 II. METHODS

### 119 A. Experimental Apparatus and Procedure

120 The angle resolved photoelectron spectra were  
121 recorded with a VG Scienta R4000 hemispherical elec-  
122 tron energy analyzer mounted on the soft X-ray undu-  
123 lator based PLÉIADES beamline at the SOLEIL syn-  
124 chrotron radiation facility (France) [17]. Comprehensive  
125 descriptions of the monochromator, electron spectrome-  
126 ter and experimental procedure have been given previ-  
127 ously [9] so only those parameters affecting the overall  
128 resolution (which is the key factor in the present study)  
129 are discussed in detail here.

130 The beamline employs an HU256 electromagnetic un-  
131 dulator which provides linearly polarized radiation in the  
132 energy range 7 — 400 eV, with the degree of polarization  
133 being estimated as  $>99\%$ . The plane of polarization can  
134 be chosen to lie either parallel or perpendicular to the  
135 plane of the electron orbit in the storage ring. Four varied  
136 line spacing, varied groove depth gratings are housed  
137 within a Petersen SX700 type monochromator [18]. The

400 lines/mm grating selected for our experiments, together with an exit slit width of 30  $\mu\text{m}$ , results in a theoretical optical resolution which varies between 1 meV at  $h\nu = 20$  eV and 4.5 meV at  $h\nu = 82$  eV. However, the actual optical resolution varied from 5 to 11 meV. This was evaluated by fitting photoelectron spectra of the  $\text{Kr}^+ (4p)^{-1} {}^2P_{3/2}$  state to deconvolute the three contributions (monochromator resolution, electron spectrometer resolution and Doppler broadening) determining the overall peak width.

The electron spectrometer was mounted in a fixed position, with photoionization occurring within a cell equipped with a series of electrodes to compensate for the so-called plasma potentials [19]. The analyser was used with a pass energy of 10 eV and a 0.2 mm curved entrance slit, resulting in a spectrometer resolution of 5 meV. The contribution  $\Delta E_D$ , due to the translational Doppler broadening, to the overall resolution is given by  $\Delta E_D = 0.7125 \sqrt{\frac{E_{KE} T}{M}}$  meV (where  $E_{KE}$  is the electron kinetic energy in eV,  $T$  is the absolute temperature of the sample gas, and  $M$  is the molecular mass expressed in atomic units [19]. For electrons ejected from bromobenzene with kinetic energies of 11 or 71 eV (corresponding to the formation of the  $\tilde{X} {}^2B_1$  state in the  $v^+ = 0$  level using photon energies of 20 or 80 eV) the translational Doppler broadening  $\Delta E_D$  is  $\sim 3.3$  or  $\sim 8.4$  meV, respectively.

Using the  $\tilde{X} {}^2B_1$  state photoelectron band as an example, the observed peak width associated with the principle vibrational progression varied between  $\sim 15$  meV at low photon energies and  $\sim 40$  meV at high photon energies. The separation between adjacent vibrational peaks was  $\sim 42$  meV. Thus, across the excitation range relevant to the present experiment the overall resolution was sufficient to allow a detailed examination of the vibrational structure. This was crucial to the extraction of vibrationally resolved photoelectron anisotropy parameters and branching ratios.

Following several freeze-pump-thaw cycles of a commercial bromobenzene sample (Sigma-Aldrich, stated purity 99.5 %), its vapour was admitted, at room temperature, into the ionization cell within the spectrometer.

At each photon energy, spectra were recorded for electrons emitted either parallel or perpendicular to the plane of polarization of the incident linearly polarized radiation. The orientation of this plane could be changed by varying the magnetic field in the undulator. Within the electric dipole approximation, and assuming randomly oriented target molecules, the photoelectron anisotropy parameter  $\beta$  associated with a particular vibrational state is given by

$$\beta = \frac{2(I_{par} - I_{perp})}{(I_{par} + 2I_{perp})} \quad (1)$$

where  $I_{par}$  and  $I_{perp}$  are the photoelectron intensities corresponding to the appropriate vibrational peak, derived from spectra recorded in the parallel and perpendicular polarization geometries, respectively.

TABLE I. Regions of photoelectron spectrum selected for analysis.

Band	From (eV)	To (eV)	Peak No.	Assignment <sup>a</sup>
$\tilde{X}$	8.965	9.008	1	0-0
	9.008	9.050	2	11 <sup>1</sup>
	9.050	9.096	3	11 <sup>2</sup>
	9.096	9.141	4	11 <sup>3</sup> , ...
	9.141	9.181	5	
	9.181	9.223	6	
$\tilde{B}$	10.578	10.663	1	0-0
	10.663	10.728	2	10 <sup>1</sup>
	10.728	10.768	3	9 <sup>1</sup>
	10.768	10.801	4	10 <sup>2</sup> , 6 <sup>1</sup>
$\tilde{C}$	11.158	11.198	1	0-0
	11.198	11.230	2	11 <sup>1</sup>
	11.230	11.276	3	
	11.276	11.318	4	
	11.318	11.348	5	

<sup>a</sup> Where shown this is the dominant transition assigned to the peak in Ref.[9]

For a particular electronic state, the vibrational branching ratio is defined as the photoelectron intensity under the selected vibrational peak divided by the summation of the photoelectron intensity in all the vibrational peaks. The evaluation of the vibrational branching ratio requires knowledge of the transmission efficiency of the electron analyzer as a function of kinetic energy. This efficiency was determined by measuring the intensity ratio between photoelectron lines with varying kinetic energies and the corresponding constant kinetic energy Auger lines [20]. This procedure was carried out at various photon energies.

Vibrationally resolved photoelectron anisotropy parameters  $\beta$  and branching ratios for the  $\tilde{X} {}^2B_1$ ,  $\tilde{B} {}^2B_2$ , and  $\tilde{C} {}^2B_1$  states were derived from the angle resolved photoelectron spectra, after normalization to the sample pressure, the photon intensity and the acquisition time (all of which were monitored during data collection), and the analyzer transmission efficiency. Table I gives the binding energy ranges used to define the vibrational members within a specific photoelectron band. The vibrational branching ratios for a particular electronic state, given here, ignore peaks due to members not relevant to the present discussion. Hence, the vibrational branching ratios for the members of interest are normalized to unity.

The software employed to determine the intensity in a particular vibrational peak simply summed the electron

counts within the binding energy range specified in Table I. No attempt was made to fit the vibrational profile. Such a procedure works well for the  $\tilde{X}$  and  $\tilde{B}$  bands where the first few vibrational peaks following that due to the adiabatic transition are dominated by contributions associated with one, or at most two, vibrational modes. It is less satisfactory for the  $\tilde{C}$  band where the vibrational structure is more complicated [9, 16].

## B. Computational Procedure

We incorporate vibrational influences into the calculation of  $\beta$  anisotropy parameters by evaluating the variation of the pure electronic dipole matrix elements with displacement of the nuclei along the vibrational coordinate. This approach has been previously used by a number of authors for the treatment of diatomic [12, 21–25] and linear triatomic [26, 27] molecular photoionization. An extension of this method to treat vibrational photoionization dynamics in polyatomic systems was recently described for a study of angular distribution parameters in chiral molecule photoionization [28], and here we adopt the same procedures to calculate  $\beta(v)$  for bromobenzene.

In this approach the vibration specific matrix elements are obtained as

$$T_{i,f,v,v^+} = \int \mathcal{X}_{i,v}(Q) M_{i,f}(Q) \mathcal{X}_{f,v^+}(Q) dQ \quad (2)$$

with the electronic matrix element, written

$$M_{i,f}(Q) = \left\langle \psi_i(\mathbf{r}; Q) \mid \hat{\eta} \mid \psi_{f,k}^{(-)}(\mathbf{r}; Q) \right\rangle_{\mathbf{r}}, \quad (3)$$

having an explicit dependence on the vibration coordinate,  $Q$ . Here  $\hat{\eta}$  is the electric dipole operator,  $\mathcal{X}_{i,v}$  and  $\mathcal{X}_{f,v^+}$  are the corresponding vibrational wavefunctions, and  $\psi_i$  and  $\psi_{f,k}^{(-)}$  are the neutral and continuum (ionized) state electronic wavefunctions. Although retaining adiabatic separation of the full vibronic functions, it is the parametric dependence of the  $\psi$ s on  $Q$  that couples electronic and nuclear motions; ignoring this dependence reverts to a FC approximation.

Harmonic normal mode vibrational analyses for the neutral and cation states were prepared using density functional theory (DFT) calculations with the B3LYP functional and cc-pVTZ basis, as implemented in the Gaussian09 package [29]. For the excited state cations, time-dependent (TD-)DFT calculations were run using the same functional and basis. The displacement of a given cation's equilibrium geometry from that of the neutral can hence be expressed in the normal mode coordinates,  $Q_m$ . A specific vibrational mode of interest,  $n$ , can then be selected for investigation, while all other modes are considered to be frozen. Using the calculated harmonic vibrational parameters and the displacement of the equilibrium geometry along  $Q_n$  it is hence possible

to expand and evaluate the associated vibrational overlap function  $\mathcal{X}_{i,v}(Q_n) \mathcal{X}_{f,v^+}(Q_n)$  appearing in Eq. 2.

The electronic matrix elements  $M_{i,f}(Q_n)$  required for Eq. 2 are obtained by CMS- $X\alpha$  calculations conducted at fixed points along  $Q_n$  with parameters chosen as previously described for fixed nuclei, equilibrium geometry calculations on bromobenzene [9]. The method for evaluating the weighted integration over  $Q_n$  (Eq. 2) has likewise been previously described [24]. Once the full matrix elements  $T_{i,f,v,v^+}$  have been obtained, the corresponding  $\beta$  values are calculated using standard formulae [30] for randomly oriented molecular targets.

## III. RESULTS

Fig. 1 shows typical photoelectron data recorded at  $h\nu = 40$  eV. Because of its relatively unstructured appearance the  $\tilde{A}$  band will not be further discussed. The  $\tilde{X}$ ,  $\tilde{B}$ , and  $\tilde{C}$  PES bands have clear vibrational structure, which was assigned [9, 16] using FC simulations (included in Fig. 1). As will be seen, these bands also possess contrasting photoelectron angular distributions:  $\tilde{X}$  ( $5b_1$  ring  $\pi$  orbital) shows no indication of a CM,  $\tilde{B}$  ( $8b_2$  Br  $4p\sigma$  in-plane lone pair orbital) displays a deep CM, while  $\tilde{C}$  ( $4b_1$  Br  $4p\pi$  lone pair orbital) has an attenuated CM due to increased interaction of this out-of-plane Br  $4p\pi$  orbital with the ring  $\pi$  orbitals [9, 10].

### A. The $\tilde{X}$ Band

Vibrationally resolved  $\tilde{X}$  band  $\beta$  parameters measured across the photon energy range 20.5 – 94 eV are shown

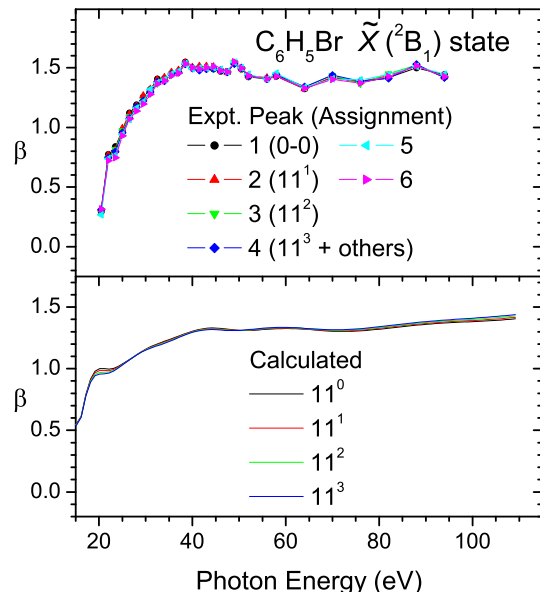


FIG. 2. Bromobenzene  $\tilde{X}$  band  $\beta(v)$ . Top: experiment; Bottom: calculations for the C-Br stretch,  $\nu_{11}$ .

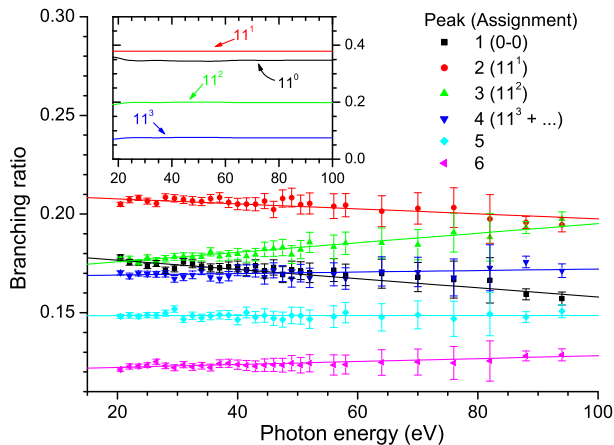


FIG. 3. Vibrational peak branching ratios for the bromobenzene  $\tilde{X}$  band. Linear best fit lines are drawn through each of the data sets. The inset shows calculated branching ratios for the  $\nu_{11} = 0-3$  transitions. Note that because of the different normalisation over 4 transitions rather than 6 peaks the absolute magnitudes are not comparable with experiment.

in Fig. 2, although hot band data has been omitted because of low intensity. The remaining peaks are predominantly a progression in the C-Br stretch,  $\nu_{11}$ , although peaks 5 and 6 are composite multiple transitions [9, 16]. Also shown in the figure are calculated  $\beta$  values for the  $\tilde{X}$  state  $\nu_{11}$  vibrational mode [31]. The clear conclusion from Fig. 2 is that  $\beta$  shows negligible experimental variation with vibrational peak, as also confirmed by the calculations.

Figure 3 shows experimental vibrational branching ratios obtained for the same  $\tilde{X}$  band peaks. These are relatively featureless, although the peak 3 intensity increases slightly with photon energy relative to peaks 1 and 2. The calculated branching ratios (inset to Fig. 3) for the individual  $\nu_{11}$  transitions are completely flat except for some weak structure at threshold. The vibrational invariance of the  $\beta$  parameters, and an energy invariance of the branching ratios, are as expected in the Franck-Condon approximation.

### B. The $\tilde{B}$ Band

Fig. 4, however, paints a different picture for the  $\tilde{B}$  band Br  $4p\sigma$  lone pair orbital. In addition to the intense Cooper Minimum, the experimental  $\beta$ s now show a distinct vibrational dependence. To better examine this, by effectively expanding the vibrational differences across the photon energy range, Fig. 4 alternatively shows  $\Delta\beta$ , the vibrational residuals relative to a common reference curve (either the experimental mean  $\beta$  or the computed  $\beta$  obtained for a fixed equilibrium geometry calculation). Around  $h\nu \approx 30$  eV, well below the obvious CM dip, a dispersion of the experimental  $\beta$ s is clear, with  $\beta(v = 0)$  spread to more positive values, the compos-

ite curve  $\beta(v_{10} = 2, v_6 = 1)$  oppositely displaced in a negative direction, and  $\beta(v_{10} = 1)$  and  $\beta(v_9 = 1)$  being intermediate. In the visual CM dip at  $h\nu \approx 70$  eV these experimental differences disappear, or possibly even reverse (unfortunately the error bars increase at higher energy because of decreasing cross-section).

These trends, including the unanticipated vibrational dependence some tens of eV below the energy of the obvious CM dip, are well captured by the calculations. In particular the dispersion of the vibrational  $\beta$ s in the 20–50 eV range is semi-quantitatively reproduced, albeit a little more structured than the experiment. The expanded insets in Fig. 4 show how the dispersion (ordering) of the vibrational  $\beta$ s switches between low and high photon energy regions, with a cross-over occurring at  $h\nu \approx 55$  eV. From the inset showing the region around 72 eV it can be seen that both the position and depth of the CM are predicted to be vibration dependent. The predicted shifts of a few eV in the minima of successive  $\nu_{10}$  vibrational levels considerably exceed the corresponding vibrational excitations. Hence these shifts are not simply attributable to consequent differences in electron energy, but must have a more fundamental origin. Furthermore, the differences evident in the  $v_9 = 1$  curve clearly suggest there is also a mode-specific behaviour in the CM dip. Unfortunately, this predicted detail cannot at present be confirmed from the experiments.

Branching ratios for the same four  $\tilde{B}$  band peaks are presented in Fig. 5. Both theory and experiment show a negligible variation with photon energy. It may be noted that although the calculated ratios differ from experiment, this may be because the estimations of the latter inevitably include contributions from multiple unresolved weak transitions and hot bands underlying the main peaks.

### C. The $\tilde{C}$ Band

The  $\tilde{C}$  state ionization of an out-of-plane Br  $4p\pi$  lone pair electron displays a weaker  $\beta$  CM. From the vibrationally unresolved electronic band measurements, it was deduced that this attenuation reflects an increased electron delocalization due to interaction with ring  $\pi$  electrons [9]. This delocalisation was evidenced in a Mulliken population analysis [8] and is similarly indicated by a reduction in the normalized electron density on the Br atom obtained in the MS-X $\alpha$  calculations conducted here (0.35 for the  $4b_1 \pi_{BrLP}$  orbital compared to 0.77 for the  $8b_2 \sigma_{BrLP}$  orbital).

Compared to the  $\tilde{X}$  and  $\tilde{B}$  states, the  $\tilde{C}$  state PES band vibrational intensities were less well reproduced by FC simulations [9, 16]. The main predicted progressions comprise excitation of the  $\nu_{11}$  C-Br stretch, either singly or in combination with the  $\nu_{10}$  mode, but relative intensities of the  $\nu_{11}$  transitions are overestimated while predicted spacings are also weakly perturbed. Consequently, it is difficult to reliably assign beyond the first adiabatic



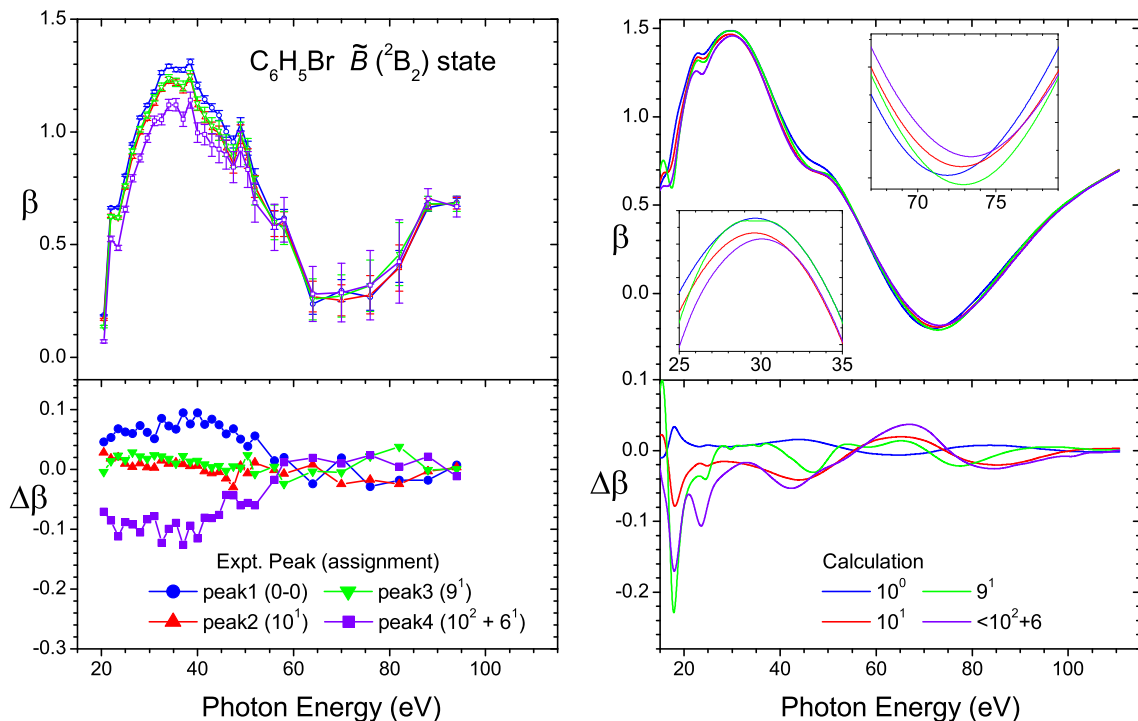


FIG. 4.  $\tilde{B}$  state vibrationally resolved  $\beta$  parameters. On the left we show experiment, on the right calculation. Two insets (top right panel) show expanded views of the maxima and minima regions of the calculated curves. For the (unresolved)  $10^2$  and  $6^1$  excitations a simple average of the individual  $10^2$  and  $6^1$  calculated  $\beta$ s is plotted. The lower panels show corresponding residuals,  $\Delta\beta$  (see text).

385 (0-0) and second ( $11^1$ ) peaks. The underlying reasons are  
 386 unclear. Palmer et al. [16] have nevertheless inferred an  
 387 absence of vibronic interaction with nearby states, given  
 388 similar vibrational line widths in the other PES bands.  
 389 However, from the better resolution in our own study [9]  
 390 it is clear that their linewidths were instrumentally lim-  
 391 ited, so this inference may not be valid.

392 Experimental branching ratios and anisotropy param-  
 393 eters,  $\beta$ , for the first five  $\tilde{C}$  band vibrational peaks are  
 394 shown in Fig. 6. While not as completely flat (constant)  
 395 as the  $\tilde{B}$  state ratios (Fig. 5) the variation of the vibra-  
 396 tional branching is quite linear across the full photon en-  
 397 ergy range, and there is again nothing to suggest a CM in-  
 398 fluenced branching behaviour. However, the vibrational  
 399 peak resolved  $\beta$  parameters again show a strong disper-  
 400 sion at energies both *below* and through the CM region,  
 401 paralleling the  $\tilde{B}$  band results in (Fig. 4).

402 These variations are more closely examined in Fig 7 by  
 403 plotting the experimental residuals,  $\Delta\beta$ , and correspond-  
 404 ing calculations that treat the two most prominent vibra-  
 405 tional modes,  $\nu_{10}, \nu_{11}$ , excited in this cationic state [9].  
 406 There is a striking similarity in the  $\beta$  dispersion in the  
 407 range 20 – 55 eV, both in experiment and the calculations  
 408 for the dominant  $\nu_{11}$  vibrational mode. At  $\sim 55$  eV both  
 409 also pass through some form of cross-over above which,  
 410 in the CM region, the  $\nu_{11}$  calculations shows structured,  
 411 oscillating  $\beta$  dispersions. In contrast the  $\nu_{10}$  calculations  
 412 show simpler behaviour, with  $\beta$ s being displaced to more

413 positive values for progressively higher vibrational excita-  
 414 tions but with no further switching of this relative order  
 415 across the 55 – 100 eV region. This looks rather more  
 416 like the experimental behaviour in the same region. Be-  
 417 low 45 eV the  $\nu_{10}$   $\beta$  curves are spread in a reversed sense,  
 418 similar now to both the  $\nu_{11}$  and the experimental results.

#### IV. CONCLUSIONS

420 At the heart of our study has been the measurement of  
 421 vibrationally resolved angular distribution  $\beta$ -parameters  
 422 and relative cross sections (branching ratios) across a  
 423 very wide photon energy range. We have examined bands  
 424 in the photoelectron spectrum of bromobenzene that dis-  
 425 play either a strong-, weak-, or no Cooper Minimum.  
 426 There is no obvious vibrational dependence of  $\beta$  for the  
 427  $\tilde{X}$  band, which lacks a CM, suggesting uncoupled elec-  
 428 tron and nuclear motion as implied by the full FC ap-  
 429 proximation.

430 For the  $\tilde{B}$  state, which has an intense, deep CM in the  
 431 photoelectron angular distribution, the calculations indi-  
 432 cate vibrational state sensitive position and depth of the  
 433 CM (Fig. 4 insets), indicative of the FC breakdown we  
 434 initially anticipated. The experimental observations con-  
 435 firm that  $\beta$  has a vibrational sensitivity in the CM region,  
 436 although unfortunately the statistical quality is insuffi-  
 437 cient to verify the specific detail that is predicted. On the

438 other hand, both the simulated and experimental vibra-  
 439 tional branching ratios are completely flat across the CM  
 440 region (Fig. 5), betraying no influence of changing dyn-  
 441 amics. Following established understanding [3, 32, 33]  
 442 such contrasting sensitivities of cross section and angu-  
 443 lar distribution can be attributed to the former's non-  
 444 dependence upon phase; implying that the  $\beta$  parameter  
 445 vibrational changes are due to varying phase of the pho-  
 446 toelectron partial waves.

447 A somewhat similar commentary may be applied to  
 448 describe the  $\tilde{C}$  state CM region results. Here, some of  
 449 the experimental branching ratios do now show a weak  
 450 linear variation with photon energy, but there is again  
 451 no structure that correlates with the visually apparent  
 452 CM dip in the  $\tilde{C}$  state  $\beta$ s. However, an unanticipated  
 453 finding for both  $\tilde{B}$  and  $\tilde{C}$  states is that the vibra-  
 454 tional dependence of the  $\beta$  parameters is even more marked  
 455 in the 20 – 50 eV photon energy range, so commencing  
 456 at energies that are well below the apparent CM energy  
 457 dip. These experimental observations are equally well  
 458 reproduced in the calculations that have been performed.

459 We thus are able to demonstrate for the first time  
 460 FC breakdown affecting photoelectron angular distribu-  
 461 tions occurring across an extended photon energy with-  
 462 out there being a resonance. On the other hand our  
 463 observations on the vibrational branching ratios do not  
 464 so directly challenge FC assumptions, at least not for the  
 465  $\tilde{B}$  state.

466 An expected prerequisite for the occurrence of the CM  
 467 in these valence bands is a strong localization of the ini-  
 468 tial orbital on the peripheral Br atom. This localization

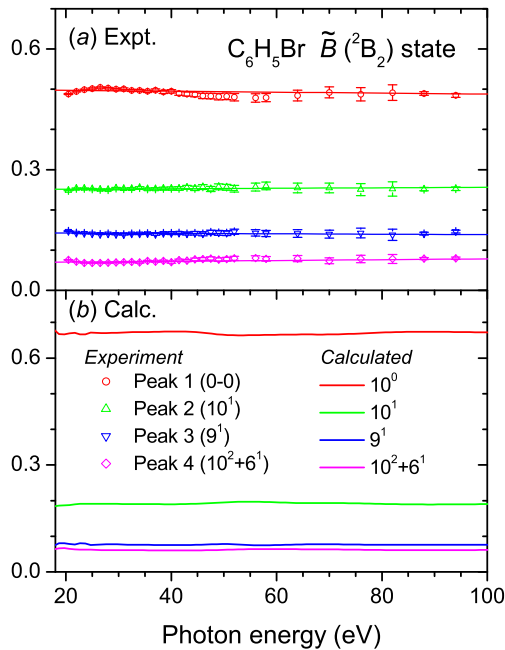


FIG. 5.  $\tilde{B}$  state vibrational branching ratios. (a) experimen-  
 tal values. The straight lines drawn through the vibrational  
 data sets are linear best fits; (b) calculated ratios.

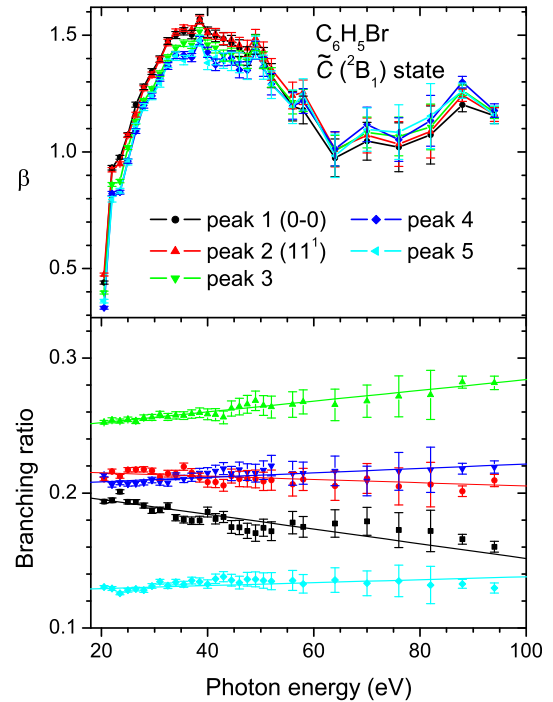


FIG. 6.  $\tilde{C}$  state  $\beta$  parameters and vibrational peak branching  
 ratios. For the latter, linear best fit straight lines are drawn  
 through each vibrational data set.

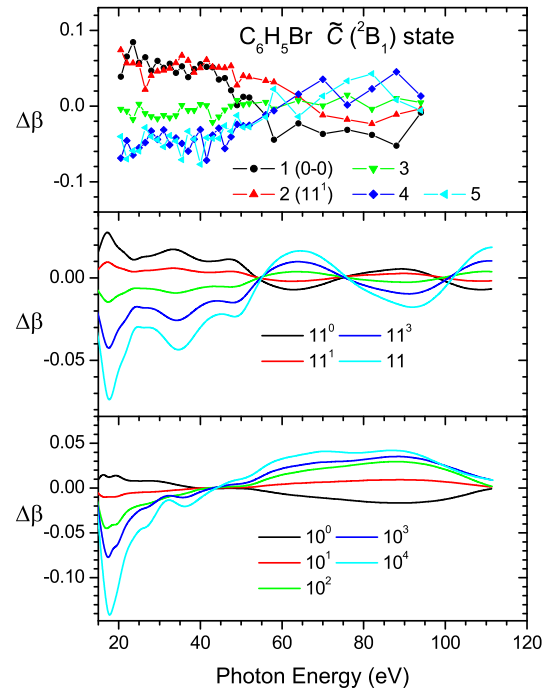


FIG. 7. (a) Experimental  $\tilde{C}$  state residuals  $\Delta\beta$  from the  
 experimental mean  $\beta$ ; (b) & (c) residuals  $\Delta\beta$  for calculated  
 excitations of  $\nu_{11}$  and  $\nu_{10}$  levels (referenced from the  $\beta$  curve  
 computed at a fixed equilibrium geometry).

469 may generally enhance the vibrational sensitivity induced  
 470 by nuclear motion (specifically that of near-neighbour  
 471 photoelectron scattering sites in the molecular ion poten-  
 472 tial), and in this sense might prove more pertinent than  
 473 just the consequent CM phenomenon, exerting influence  
 474 across an even wider energy range. Nevertheless, both  
 475 the  $\tilde{B}$  band (Fig. 4 insets) and, especially, the  $\tilde{C}$  band  
 476 (Fig. 7) results hint at unexpected patterns of vibrational  
 477 *mode*-specific variation in the region of the actual CM dip  
 478 that are not yet understood and merit further investiga-

479 tion.

## ACKNOWLEDGMENTS

481 This research was funded by the European Com-  
 482 munity's Seventh Framework Program (FP7/2007-2013)  
 483 ELISA under grant agreement no. 226716. We are grate-  
 484 ful to SOLEIL staff for running the facility and providing  
 485 beamtime (Project 20120162).

- 
- 486 [1] A. D. Shiner, B. E. Schmidt, C. Trallero-Herrero, P. B.  
 487 Corkum, J. C. Kieffer, F. Legare, and D. M. Villeneuve,  
 488 J. Phys. B : At. Mol. Opt. Phys. **45**, 074010 (2012);  
 489 M. Ruberti, V. Averbukh, and P. Decleva, J. Chem.  
 490 Phys. **141**, 164126 (2014); S. B. Schoun, R. Chirla,  
 491 J. Wheeler, C. Roedig, P. Agostini, L. F. DiMauro, K. J.  
 492 Schafer, and M. B. Gaarde, Phys. Rev. Lett. **112**, 153001  
 493 (2014); F. Cloux, B. Fabre, and B. Pons, Phys. Rev. A  
 494 **91**, 023415 (2015).
- 495 [2] J. W. Cooper, Phys. Rev. **128**, 681 (1962).
- 496 [3] U. Becker and D. Shirley, "Partial cross sections and an-  
 497 gular distributions," in *VUV and Soft X-Ray Photoion-*  
 498 *ization*, edited by U. Becker and D. A. Shirley (Plenum,  
 499 New York, 1996) Chap. 5, pp. 135–180.
- 500 [4] T. A. Carlson, M. O. Krause, W. A. Svensson, P. Gerard,  
 501 F. A. Grimm, T. A. Whitley, and B. P. Pullen, Z. Phys.  
 502 D: Atoms, Molecules and Clusters **2**, 309 (1986).
- 503 [5] M. C. H. Wong, A. T. Le, A. F. Alharbi, A. E. Bog-  
 504 uslavskiy, R. R. Lucchese, J. P. Brichta, C. D. Lin, and  
 505 V. R. Bhardwaj, Phys. Rev. Lett. **110**, 033006 (2013).
- 506 [6] T. A. Carlson, A. Fahlman, M. O. Krause, T. A. Whitley,  
 507 and F. A. Grimm, J. Chem. Phys. **81**, 5389 (1984).
- 508 [7] I. Powis, J. D. Thrower, A. B. Trofimov, T. E.  
 509 Moskovskaya, J. Schirmer, A. W. Potts, D. M. P. Hol-  
 510 land, F. Bruhn, and L. Karlsson, Chem. Phys. **315**,  
 511 121 (2005); I. Powis, I. L. Zaytseva, A. B. Trofimov,  
 512 J. Schirmer, D. M. P. Holland, A. W. Potts, and L. Karls-  
 513 son, J. Phys. B: At. Mol. Opt. Phys. **40**, 2019 (2007).
- 514 [8] M. Schneider, D. Y. Soshnikov, D. M. P. Holland,  
 515 I. Powis, E. Antonsson, M. Patanen, C. Nicolas,  
 516 C. Miron, M. Wormit, A. Dreuw, and A. B. Trofimov,  
 517 J. Chem. Phys. **143**, 144103 (2015).
- 518 [9] I. Powis, D. M. P. Holland, E. Antonsson, M. Patanen,  
 519 C. Nicolas, C. Miron, M. Schneider, D. Y. Soshnikov,  
 520 A. Dreuw, and A. B. Trofimov, J. Chem. Phys. **143**,  
 521 144304 (2015).
- 522 [10] D. M. P. Holland, D. Edvardsson, L. Karlsson,  
 523 R. Maripuu, K. Siegbahn, A. W. Potts, and W. von  
 524 Niessen, Chem. Phys. **252**, 257 (2000).
- 525 [11] K. H. Wang, J. A. Stephens, and V. McKoy, J. Phys.  
 526 Chem. **98**, 460 (1994).
- 527 [12] J. A. Stephens and V. McKoy, Phys. Rev. Lett. **62**, 889  
 528 (1989).
- 529 [13] K. Wang, J. A. Stephens, and V. McKoy, J. Chem. Phys.  
 530 **95**, 6456 (1991).
- 531 [14] J. B. Bertrand, H. J. Worner, P. Hockett, D. M. Vil-  
 532 leneuve, and P. B. Corkum, Phys. Rev. Lett. **109**, 143001  
 533 (2012).
- 534 [15] R. M. Rao, E. D. Poliakov, K. H. Wang, and V. McKoy,  
 535 Phys. Rev. Lett. **76**, 2666 (1996); J. Chem. Phys. **104**,  
 536 9654 (1996); J. A. Lopez-Dominguez, D. Hardy, A. Das,  
 537 E. D. Poliakov, A. Aguilar, and R. R. Lucchese, J. Elec.  
 538 Spectrom. Rel. Phen. **185**, 211 (2012).
- 539 [16] M. H. Palmer, T. Ridley, S. V. Hoffmann, N. C. Jones,  
 540 M. Coreno, M. de Simone, C. Grazioli, T. Zhang,  
 541 M. Biczysko, A. Baiardi, and K. Peterson, J. Chem.  
 542 Phys. **143**, 164303 (2015).
- 543 [17] J. Söderström, A. Lindblad, A. N. Grum-Grzhimailo,  
 544 O. Travnikova, C. Nicolas, S. Svensson, and C. Miron,  
 545 New J. Phys. **13**, 073014 (2011).
- 546 [18] H. Petersen, Opt. Comm. **40**, 402 (1982).
- 547 [19] P. Baltzer, L. Karlsson, M. Lundqvist, and B. Wannberg,  
 548 Rev. Sci. Instrum. **64**, 2179 (1993).
- 549 [20] J. Jauhainen, A. Ausmees, A. Kivimäki, S. J. Osborne,  
 550 A. N. Debrito, S. Aksela, S. Svensson, and H. Aksela, J.  
 551 Elec. Spect. and Rel. Phen. **69**, 181 (1994).
- 552 [21] D. A. Mistrov, A. De Fanis, M. Kitajima, M. Hoshino,  
 553 H. Shindo, T. Tanaka, Y. Tamenori, H. Tanaka, A. A.  
 554 Pavlychev, and K. Ueda, Phys. Rev. A **68**, 022508  
 555 (2003).
- 556 [22] S. K. Semenov, N. A. Cherepkov, T. Jahnke, and  
 557 R. Dorner, J. Phys. B: At. Mol. Opt. Phys. **37**, 1331  
 558 (2004).
- 559 [23] M. Hoshino, R. Montuoro, R. R. Lucchese, A. De Fanis,  
 560 U. Hergenbahn, G. Prumper, T. Tanaka, H. Tanaka, and  
 561 K. Ueda, J. Phys. B: At. Mol. Opt. Phys. **41**, 085105  
 562 (2008).
- 563 [24] I. Powis, Phys. Rev. A **84**, 013402 (2011).
- 564 [25] E. Plesiat, P. Decleva, and F. Martin, Phys. Chem.  
 565 Chem. Phys. **14**, 10853 (2012).
- 566 [26] R. R. Lucchese, J. Soderstrom, T. Tanaka, M. Hoshino,  
 567 M. Kitajima, H. Tanaka, A. De Fanis, J. E. Rubensson,  
 568 and K. Ueda, Phys. Rev. A **76**, 012506 (2007).
- 569 [27] A. Das, E. D. Poliakov, R. R. Lucchese, and J. D. Bozek,  
 570 J. Chem. Phys. **130**, 044302 (2009).
- 571 [28] G. A. Garcia, H. Dossmann, L. Nahon, S. Daly, and  
 572 I. Powis, ChemPhysChem **18**, 500 (2017).
- 573 [29] M. J. Frisch, G. W. Trucks, H. B. Schlegel, G. E. Scuseria,  
 574 M. A. Robb, J. R. Cheeseman, G. Scalmani, V. Barone,  
 575 B. Mennucci, G. A. Petersson, H. Nakatsuji, M. Caric-  
 576 cato, X. Li, H. P. Hratchian, A. F. Izmaylov, J. Bloino,  
 577 G. Zheng, J. L. Sonnenberg, M. Hada, M. Ehara, K. Toy-  
 578 ota, R. Fukuda, J. Hasegawa, M. Ishida, T. Nakajima,  
 579 Y. Honda, O. Kitao, H. Nakai, T. Vreven, J. J. A. Mont-  
 580 gomery, J. E. Peralta, F. Ogliaro, M. Bearpark, J. J.  
 581 Heyd, E. Brothers, K. N. Kudin, V. N. Staroverov,



- 582 T. Keith, R. Kobayashi, J. Normand, K. Raghavachari, 594  
583 A. Rendell, J. C. Burant, S. S. Iyengar, J. Tomasi, 595  
584 M. Cossi, N. Rega, J. M. Millam, M. Klene, J. E. 596  
585 Knox, J. B. Cross, V. Bakken, C. Adamo, J. Jaramillo, 597  
586 R. Gomperts, R. E. Stratmann, O. Yazyev, A. J. Austin, 598  
587 R. Cammi, C. Pomelli, J. W. Ochterski, R. L. Martin, 599  
588 K. Morokuma, V. G. Zakrzewski, G. A. Voth, P. Sal- 600  
589 vador, J. J. Dannenberg, S. Dapprich, A. D. Daniels, 601  
590 O. Farkas, J. B. Foresman, J. V. Ortiz, J. Cioslowski, 602 [32] J. Cooper and R. N. Zare, *J. Chem. Phys.* **48**, 942 (1968).  
591 and D. J. Fox, "Gaussian 09 revision d.01," (2013). 603 [33] D. Dill, *Phys. Rev. A* **7**, 1976 (1973).
- 592 [30] D. Dill and J. L. Dehmer, *J. Chem. Phys.* **61**, 692 (1974).  
593 [31] The notation  $m^n$  as used here indicates vibrational mode,  $m$ , and level,  $n$ , excited in the ion. For experiment the adiabatic (vibrationless) excitations are alternatively labelled "0-0" but for the calculated quantities we retain the notation  $m^0$  since while zero point motion of the mode  $m$  is included, all other modes are considered frozen. Hence calculations for the nominally vibrationless excitation of the ion may nevertheless have some dependence on the selected mode,  $m$ .

